ACADEMIC PRESS

Available online at www.sciencedirect.com

SCIENCE DIRECT®

Journal of Computational Physics 185 (2003) 375–398

JOURNAL OF COMPUTATIONAL PHYSICS

www.elsevier.com/locate/jcp

A blended pressure/density based method for the computation of incompressible and compressible flows

C.-C. Rossow *

DLR, Deutsches Zentrum für Luft- und Raumfahrt, Institut für Aerodynamik und Strömungstechnik, 38022 Braunschweig, Germany

Received 23 April 2001; received in revised form 11 November 2002; accepted 28 November 2002

Abstract

An alternative method to low speed preconditioning for the computation of nearly incompressible flows with compressible methods is developed. For this approach the leading terms of the flux difference splitting (FDS) approximate Riemann solver are analyzed in the incompressible limit. In combination with the requirement of the velocity field to be divergence-free, an elliptic equation to solve for a pressure correction to enforce the divergence-free velocity field on the discrete level is derived. The pressure correction equation established is shown to be equivalent to classical methods for incompressible flows. In order to allow the computation of flows at all speeds, a blending technique for the transition from the incompressible, pressure based formulation to the compressible, density based formulation is established. It is found necessary to use preconditioning with this blending technique to account for a remaining "compressible" contribution in the incompressible limit, and a suitable matrix directly applicable to conservative residuals is derived. Thus, a coherent framework is established to cover the discretization of both incompressible and compressible flows. Compared with standard preconditioning techniques, the blended pressure/density based approach showed improved robustness for high lift flows close to separation.

Keywords: Incompressible and compressible flows; Navier–Stokes equations; Riemann problem; Pressure correction method; Low speed preconditioning

1. Introduction

Computational methods used in aerospace applications for the computation of compressible flows have reached a very high level of maturity with respect to accuracy and efficiency, e.g., [1–6]. However, many aerodynamic problems solved today involve mixed compressible and incompressible flow regions, especially when considering the flow around the high lift system of aircraft. In order not to sacrifice the mature basis established with such codes, it is therefore highly desirable to extend these methods towards the incompressible flow regime. Usually, in compressible codes also for steady flow problems the unsteady equations

* Tel.: +49-531-295-2410; fax: +49-531-295-2320.
E-mail address: cord.rossow@dlr.de

0021-9991/02/$ - see front matter
doi:10.1016/S0021-9991(02)00059-1

are solved as a coupled system in strong conservation form and integrated towards steady state. To achieve the extension to the solution of low Mach number flows, the time derivatives of the system of compressible equations are multiplied by a suitable preconditioning matrix [7–9]. However, in regions of very low Mach number, e.g., near stagnation points and in recirculation regions, the preconditioning matrix may become singular [10], and the robustness of the computation may be impaired [11]. Therefore, to make compressible codes applicable to incompressible flow problems with the same reliability as for compressible cases, further effort seems to be required to understand the basic mechanisms of computing incompressible flows with methods originally designed for compressible flows.

During the ongoing quest for computational methods being capable to compute flows at all speeds, also the other alternative, namely to extend classical incompressible, pressure based methods to the compressible flow regime, is under extensive research [12–18]. In the pressure based approach, staggered [12,16] as well as colocated [13–15,17,18] locations of variables are employed. The equations are often solved in an uncoupled manner using a scalar transport equation for temperature [12,13,17] or enthalpy [16]. In [17] a special procedure ensures that when using a scalar transport equation for temperature the discrete conservation law is still satisfied exactly, and when the flow becomes compressible the discretization of the governing equations is reverted to a scheme frequently used in compressible flow solvers [19]. In other methods constant enthalpy flow is assumed and the energy equation is dropped [14,18], as was also done in [13] for the inviscid flow cases computed. However, in aerospace applications the strong conservation form is regarded as being of paramount importance to ensure reliable and accurate capturing of all relevant flow features, and for viscous flows the assumption of constant enthalpy is in general not valid. With regard to complex configurations, the staggered approach seems less attractive, and switching from one discretization scheme to another may also lead to conceptual difficulties.

In the present work, a method will be developed which allows application to both compressible and incompressible flows. As a basis, the MAPS+ flux splitting scheme developed in [20] will be used. The derivation of the MAPS+ discretization was based on the extension of the flux difference splitting (FDS) [19] scheme in terms of Mach number. This extension allowed to distinguish between terms relevant in the compressible flow regime and terms dominant in the incompressible limit. It was shown in [20] that mainly appropriately scaled pressure differences form the dissipative terms in the incompressible limit. In the present work, these pressure differences are used to derive an equation for pressure such that a divergence-free velocity field may be established for the discrete equations. Parallels to classical incompressible pressure correction methods on colocated meshes [21] will be drawn. The formulation proposed in this work leads to a consistent framework covering the classical pressure correction approach for incompressible flows and the density based compressible methods, with the whole derivation relying on the approximate solution of the Riemann problem. The performance of the present method will be assessed by computing steady incompressible and compressible, inviscid and viscous flow around airfoils.

2. Governing equations

We consider the two-dimensional Navier–Stokes equations for compressible flow. The system of partial differential equations in strong conservation form is given by

$$\frac{\partial \vec{W}}{\partial t} + \frac{\partial \vec{F}^x}{\partial x} + \frac{\partial \vec{F}^y}{\partial y} = 0, \tag{1}$$

where $\vec{W}$ represents the vector of conservative variables, and $\vec{F}^x, \vec{F}^y$ denote the flux-density vectors for the x and y directions, respectively. Setting the viscous parts of the flux-density tensor to zero, the Euler equations governing inviscid flow are obtained

$$\begin{aligned}
&\frac{\partial \rho}{\partial t} + \frac{\partial(\rho u)}{\partial x} + \frac{\partial(\rho v)}{\partial y} = 0,\\
&\frac{\partial(\rho u)}{\partial t} + \frac{\partial(\rho u^2 + p)}{\partial x} + \frac{\partial(\rho uv)}{\partial y} = 0,\\
&\frac{\partial(\rho v)}{\partial t} + \frac{\partial(\rho uv)}{\partial x} + \frac{\partial(\rho v^2 + p)}{\partial y} = 0,\\
&\frac{\partial(\rho E)}{\partial t} + \frac{\partial(\rho uH)}{\partial x} + \frac{\partial(\rho vH)}{\partial y} = 0,
\end{aligned} \tag{2}$$

where x and y denote the cartesian coordinates, and ρ, u, v, E, p, H, represent density, cartesian velocity components, specific total energy, pressure, and specific total enthalpy, respectively. In order to close this system, the equation of state

$$\frac{p}{\rho} = R \cdot T \tag{3}$$

is used with R as specific gas constant and T as temperature. Furthermore, the speed of sound for compressible, isentropic flow is defined by Laplace's equation

$$\frac{\mathrm{d}p}{\mathrm{d}\rho} = c^2. \tag{4}$$

Approaching the incompressible flow regime, changes in the density of a fluid particle become negligible, and the energy equation decouples from the fluid flow problem. To solve for incompressible flows, in conservation form one is left with the set of equations

$$\begin{aligned}
&\frac{\partial(\rho u)}{\partial x} + \frac{\partial(\rho v)}{\partial y} = 0,\\
&\frac{\partial(\rho u)}{\partial t} + \frac{\partial(\rho u^2 + p)}{\partial x} + \frac{\partial(\rho uv)}{\partial y} = 0,\\
&\frac{\partial(\rho v)}{\partial t} + \frac{\partial(\rho uv)}{\partial x} + \frac{\partial(\rho v^2 + p)}{\partial y} = 0.
\end{aligned} \tag{5}$$

Comparing Eq. (5) to Eq. (2), it is obvious that, as noted above, the energy equation has been dropped. However, the major difference in these two sets of equations is that the time derivative of density in the continuity equation has disappeared. As a consequence, the original system of equations (2) is no longer hyperbolic with respect to time. For incompressible flow as given by Eq. (5), the continuity equation acts as a constraint which has to be respected, regardless whether the flow is steady or unsteady. It is essentially this constraint which changes the character of the equations from purely hyperbolic in time to elliptic, since it is supposed to hold at all times instead of being approached by marching in time-direction. In the incompressible limit, the material derivative of density becomes zero, and the continuity equation in Eq. (5) becomes the requirement that the velocity field $\vec{q}$ has to be divergence-free

$$\mathrm{div}(\vec{q}) = \frac{\partial u}{\partial x} + \frac{\partial v}{\partial y} = 0, \quad \vec{q} = \begin{bmatrix} u \\ v \end{bmatrix}. \tag{6}$$

3. Derivation of the pressure correction equation

In the discussion of the governing equations, it was pointed out that for incompressible flow the continuity equation becomes a constraint to be respected at all times, stating that the velocity field $\vec{q}$ must be divergence-free, Eq. (6). Applying preconditioning techniques such as [7–9], this constraint is not generally respected. The preconditioning matrices are purely a mathematical means to reduce the stiffness of the system of equations by changing the eigenvalues. This is mainly achieved by introducing an artificial speed of sound which is in the order of the mean flow speed. In [7,22] it was outlined that this artificial speed of sound also leads to the proper scaling of the artificial dissipation for incompressible flows. After preconditioning the equations, time-marching is used to integrate towards the steady state. However, there is no guarantee that the time-marching process, during which the velocity field may not be divergence-free, reaches a steady, divergence-free state. In practice, robustness problems occur with this technique for complex flows. Regarding the discussion of the governing equations in the incompressible limit, it may be noticed that the introduction of the artificial speed of sound to reduce the stiffness of the system of equations is not supported by the physics of the flow: acoustic disturbances are supposed to travel infinitely fast compared to the flow speed, leading to the fulfillment of the divergence-free constraint. Thus, it may be suspected that the disregard of the divergence-free constraint is a source for the robustness problems encountered when using low speed preconditioning. Therefore, in the present work attention is focused on the question whether there is a way to respect the divergence-free constraint on the discrete level when solving for incompressible flows.

In the following, the discrete mass flux obtained from the application of FDS [19] will be analyzed with respect to the establishment of a divergence-free velocity field. Using the basic FDS scheme of [19], the inviscid flux density vector $\vec{F}$ normal to a cell interface may be written as

$$\vec{F} = \frac{1}{2}\left(\vec{F}^{\mathrm{L}} + \vec{F}^{\mathrm{R}}\right) - \frac{1}{2}\left|\overline{\overline{A}}\right|\Delta\vec{W}, \tag{7}$$

where $\vec{F}^{\mathrm{L}}$ and $\vec{F}^{\mathrm{R}}$ are the left and right states of the inviscid flux density vector normal to the cell interface, $\overline{\overline{A}}$ is the corresponding flux Jacobian, and $\Delta\vec{W}$ denotes the differences in conservative variables between left and right states of a cell interface. In [20], the expression $|\overline{\overline{A}}| \cdot \Delta\vec{W}$ was expanded in terms of the interface Mach number M_0, with M_0 defined as

$$M_0 = \min(|M|, 1) \cdot \mathrm{sign}(M). \tag{8}$$

Following [20], the resulting expressions of $|\overline{\overline{A}}| \cdot \Delta\vec{W}$ are summarized in Table 1 as flux differences $\Delta\vec{F}$ for the continuity, momentum, and energy equations. As outlined in [20], for compressible flows the terms scaled linearly with $|M_0|$ become dominant, whereas for incompressible flows these terms vanish and all terms scaled by $(1 - |M_0|)$ dominate. Note that in order to obtain the proper scaling of the numerical dissipation

Table 1
Flux difference splitting dissipation expanded in Mach number

$\Delta F_{\rho} = \frac{1}{c}(1 - \lvert M_0\rvert)\Delta p + \rho\lvert M_0\rvert\Delta q_n + \lvert q_n\rvert\Delta\rho$
$\Delta F_{\rho u} = n_x\lvert M_0\rvert\Delta p + \frac{1}{c}u(1 - \lvert M_0\rvert)\Delta p + n_x\rho c(1 - \lvert M_0\rvert)\Delta q_n + \rho u\lvert M_0\rvert\Delta q_n + \lvert q_n\rvert\Delta\rho u$
$\Delta F_{\rho v} = n_y\lvert M_0\rvert\Delta p + \frac{1}{c}v(1 - \lvert M_0\rvert)\Delta p + n_y\rho c(1 - \lvert M_0\rvert)\Delta q_n + \rho v\lvert M_0\rvert\Delta q_n + \lvert q_n\rvert\Delta\rho v$
$\Delta F_{\rho H} = \frac{1}{c}H(1 - \lvert M_0\rvert)\Delta p - \lvert q_n\rvert(1 - \lvert M_0\rvert)\Delta p + q_n\rho c(1 - \lvert M_0\rvert)\Delta q_n + \rho H\lvert M_0\rvert\Delta q_n + \lvert q_n\rvert\Delta\rho H$

in the incompressible limit, the speed of sound c in Table 1 has to be replaced by an artificial speed of sound c', which is of the order of the mean flow speed [7,20,22]. Thus, the dominance of the pressure differences scaled by $(1/c')(1-|M_0|)$ is strongly amplified in these cases. From Eq. (7) and the expressions of Table 1 the discrete mass flux density at a cell face S can be computed as

$$F^{\rho} = \frac{1}{2}\cdot\left[\left(\rho q_n^{\mathrm{L}} + \rho q_n^{\mathrm{R}}\right) - \frac{1}{c'}(1-|M_o|)\Delta p + \mathrm{ODT}\right], \tag{9}$$

where q_{n} denotes the velocity normal to the cell interface defined as $q_{\mathrm{n}} = \vec{q}\cdot\vec{n}$ with $\vec{n}$ as the outward facing normal of cell face S, and ODT stands for other dissipative terms as listed in Table 1. The pressure difference Δp denotes the difference between values on the left side L and right side R at a cell interface, giving $\Delta p = p^{\mathrm{R}} - p^{\mathrm{L}}$, where the normal vector $\vec{n}$ at a cell interface is pointing from left to right when the cell boundary is traversed in a mathematically positive sense. The corresponding discrete mass flux through the cell face is obtained by multiplying Eq. (9) by the cell face area S:

$$F^{\rho}\cdot S = \frac{1}{2}\cdot\left[\left(\rho q_n^{\mathrm{L}} + \rho q_n^{\mathrm{R}}\right) - \frac{1}{c'}(1-|M_0|)\Delta p + \mathrm{ODT}\right]\cdot S. \tag{10}$$

Note that the term $(1/c')(1-|M_0|)\Delta p$ comprises the acoustic part of the crossflow diffusion terms identified in [20]. In [20], it was the importance of the shear waves in the crossflow diffusion which was pointed out, whereas in the following it will be these acoustic terms which will be used to derive the pressure correction equation.

Using the FDS discretization of [19] to obtain the intermediate state at cell interfaces, the discrete divergence of $\rho\vec{q}$ in a cell is expressed as

$$\mathrm{div}(\rho\vec{q}) = \frac{1}{\mathrm{vol}}\cdot\sum_{i=1}^{i\mathrm{faces}} F_i^{\rho}\cdot S_i = \frac{1}{\mathrm{vol}}\cdot\sum_{i=1}^{i\mathrm{faces}}\frac{1}{2}\cdot\left[\left(\rho q_n^{\mathrm{L}} + \rho q_n^{\mathrm{R}}\right) - \frac{1}{c'}(1-|M_0|)\Delta p + \mathrm{ODT}\right]_i\cdot S_i, \tag{11}$$

where "ifaces" denotes the number of faces of the computational cell with "i" as the running index, and "vol" is the cell volume.

For constant density flows, Eq. (11) is equivalent to the discrete divergence of velocity times a constant, and a divergence-free velocity field may be established if a pressure correction p' is introduced such that

$$\mathrm{div}(\rho\vec{q}) = \frac{1}{\mathrm{vol}}\cdot\sum_{i=1}^{i\mathrm{faces}}\frac{1}{2}\cdot\left[\left(\rho q_n^{\mathrm{L}} + \rho q_n^{\mathrm{R}}\right) - \frac{1}{c'}(1-|M_0|)\left(\Delta p + \Delta p'\right) + \mathrm{ODT}\right]_i\cdot S_i = 0, \tag{12}$$

where for the differences $\Delta p'$ the same conventions hold as in Eqs. (9) and (10) for Δp. Eq. (12) is an elliptic equation for the correction of pressure to fulfill $\mathrm{div}(\rho\vec{q}) = 0$ on the discrete level. Rearrangement of Eq. (12) leads to

$$\begin{aligned}\sum_{i=1}^{i\mathrm{faces}}\frac{1}{2}\cdot\left[\frac{1}{c'}(1-|M_0|)\Delta p'\right]_i\cdot S_i &= \sum_{i=1}^{i\mathrm{faces}}\frac{1}{2}\cdot\left[\left(\rho q_n^{\mathrm{L}} + \rho q_n^{\mathrm{R}}\right) - \frac{1}{c'}(1-|M_0|)\Delta p + \mathrm{ODT}\right]_i\cdot S_i \\ &= \mathrm{vol}\cdot\mathrm{Res}[\rho],\end{aligned} \tag{13}$$

where $\mathrm{Res}[\rho]$ represents the residual obtained using the preconditioned FDS discretization of Eq. (7) and Table 1 to spatially discretize the continuity equation in Eq. (2). The computation of $\mathrm{Res}[\rho]$ is therefore identical to the usual way the residual of the continuity equation is computed in compressible codes using the FDS discretization in combination with low speed preconditioning, where the artificial speed of sound c' is introduced. Having solved Eq. (13) for the pressure correction p', the pressure field may be updated by

$$p^{\text{new}} = p^{\text{old}} + p'. \tag{14}$$

Note that the pressure correction equation (13) was directly derived from the approximate solution of the Riemann problem using the terms of Table 1. The solution of the Riemann problem reflects the information propagation in the flow field and guides how to construct the intermediate state at a cell interface with respect to the flow physics. The discrete problem enters the derivation via the scaling of the pressure differences by the artificial speed of sound c'. As outlined in [22], this scaling is required since the discrete equations support pressure disturbances of $O(M)$, in contrast to the analytical equations which only support $O(M^2)$ disturbances.

4. Parallels to classical pressure correction schemes

The formulation derived above bears a strong resemblance to classical pressure correction schemes used to solve for incompressible flows. One of the most prominent representatives of this class of methods is the SIMPLE (semi-implicit pressure linked equations) scheme of Patankar [23]. Without going into detail, following the textbook of Hirsch [24] the equation to solve for the pressure correction reads

$$|\vec{\nabla}^2|p' = \frac{1}{\Delta t}\vec{\nabla}\vec{q}, \tag{15}$$

where

$$\vec{\nabla} = \begin{bmatrix} \partial/\partial x \\ \partial/\partial y \end{bmatrix}, \quad \Delta t \approx \frac{\Delta x}{|q|}. \tag{16}$$

Note that the scaling in Eq. (15) by Δt corresponds to the scaling in Eq. (13) with an artificial speed of sound of the order of the mean flow velocity.

The SIMPLE scheme of [23] was developed using staggered meshes, and Rhie and Chow [21] implemented the pressure correction method on colocated meshes. In order to avoid pressure/velocity decoupling, the mass flux density through a cell interface is augmented by pressure differences to yield [17]

$$F^{\rho} = \frac{1}{2}\left(\rho q_n^{\mathrm{L}} + \rho p_n^{\mathrm{R}}\right) - \frac{\text{vol}}{f(\rho, q, \mu, S)}\left[\frac{p^{\mathrm{R}} - p^{\mathrm{L}}}{ds} - \frac{1}{2}\left(\vec{\nabla}p^{\mathrm{L}} + \vec{\nabla}p^{\mathrm{R}}\right)\cdot\vec{e}_s\right], \tag{17}$$

where ds is the distance between the centers of the left and right cell, $\vec{e}_s$ is the unit vector pointing in the direction of the line connecting the left and right cell center, and $f(\rho, q, \mu, S)$ is a function scaling the pressure dissipation. This scaling is of the same order of magnitude as the scaling in Eq. (9) introduced by the artificial speed of sound in the case of incompressible flows. In order to understand the pressure dissipation terms in Eq. (17), it must be remembered that usually in classical pressure correction methods the values for pressure at the left and right sides of the interface are not reconstructed via extrapolation as done in compressible codes, but p^{L} and p^{R} in Eq. (17) are directly taken from the left and right cell center. As was shown in [25] and also exploited in [14,18], the pressure terms in Eq. (17) lead to dissipative terms comprised of fourth differences of pressure, scaled inversely by terms of $O(q, \mu)$. This pressure differences dissipation in the mass flux density is thus similar to the pressure differences dissipation found in the mass flux density given by Eq. (9) using the artificial speed of sound c': in compressible codes, p^{L} and p^{R} are reconstructed by extrapolation to obtain second order accuracy, and the differences of the reconstructed values lead to a fourth differences dissipative operator [26]. Using the artificial speed of sound as with preconditioning in Eq. (9), the scaling is similar to Eq. (17), with the exception that the influence of the dynamic viscosity μ is neglected.

Further insight into the similarity of classical colocated pressure correction methods and the present approach can be gained with regard to what is called the "correction to the cell face velocity" in colocated pressure correction methods [21,27]: the term $-[\mathrm{vol}/(f(\rho,q,\mu,S))][(p^{\mathrm{R}}-p^{\mathrm{L}})/ds]$ in Eq. (17) of the classical, colocated pressure correction approach is the counterpart to the term $-(1/c')(1-|M_0|)\Delta p$ of the present method, which was derived from the approximate solution of the Riemann problem. Introducing a pressure correction p', this leads for the present method to a term $-(1/c')(1-|M_0|)\Delta p'$, see Eq. (13), and for the classical pressure correction equation it yields the term

$$-\frac{\mathrm{vol}}{(f(\rho,q,\mu,S))}\frac{p'^{\mathrm{R}}-p'^{\mathrm{L}}}{ds}.$$

This expression is similar to what is called in colocated pressure correction schemes the "correction to the cell face velocity" [27]. The equation for the "correction to the cell face velocity", employing the usual "compass" notation of pressure correction literature, reads [27]

$$u'_{\mathrm{e}} = -S_{\mathrm{e}}\overline{\left(\frac{1}{A_p^u}\right)}_{\mathrm{e}}(p'_{\mathrm{E}}-p'_{\mathrm{P}}), \tag{18}$$

where the index "e" denotes the "east" cell face between cell center P to the left and cell center E to the right, S_{e} is the corresponding cell face area, and A_p^u is the scaling coefficient. Interpreting the dissipative terms derived from the approximate solution of the Riemann problem in the same way as in colocated pressure correction schemes, also in the present method a "correction to the cell face velocity " is established. Note that for pressure correction schemes suited for incompressible and compressible flows, however not velocity but mass flux is "corrected" to ensure mass conservation, see e.g. [21,27]. This is identical to the procedure resulting from the present method.

Thus, from the explanations above, two conclusions can be drawn. First, the formulation for a pressure correction equation derived in this work is similar to the pressure correction equation of classical incompressible methods. In [23], the pressure correction equation is derived from the discrete equations using truncated momentum equations to obtain discrete velocity corrections, and introducing these velocity corrections into the discrete continuity equation leads to the pressure correction equation. In contrast to that, in the present investigation, the pressure correction equation was directly derived from the approximate solution of the Riemann problem to respect the constraint of the divergence-free velocity field. The second conclusion is that the pressure dissipation introduced by Rhie and Chow [21] in order to prevent pressure/velocity decoupling on colocated meshes is not an arbitrary means, but these terms can be consistently derived from the solution of a Riemann problem at low Mach number, scaled using the artificial speed of sound c' to establish the correct damping behavior [22].

5. Implementation of the pressure correction equation for incompressible flows

The pressure correction approach derived above has been implemented in the 3D unstructured, compressible finite volume NOUGAT (node oriented unstructured generic algorithm testing) code. NOUGAT serves as a research basis for the DLR-τ code and uses identical geometrical preprocessing as the τ code [3]. Thus, the NOUGAT code is a node based scheme using dual mesh metrics. Deviating from the τ code, the spatial discretization in NOUGAT is based on the MAPS+ flux splitting scheme [20], and least squares gradients are used for second order reconstruction [28,29]. Time integration is achieved by an explicit 5-stage Runge–Kutta scheme, and convergence towards steady state is accelerated by local time stepping, agglomeration multigrid, and an implicit residual smoothing technique based on the MAPS+ formulation

[30]. The influence of turbulence is taken into account employing the one-equation model of Spalart and Allmaras [31], following the implementation of [3]. Usually, CFL-numbers of six are employed, and convergence rates similar to structured codes with Runge–Kutta timestepping and multigrid are achieved [20,30].

To respect the constraint of a divergence-free velocity field for incompressible flows, the pressure correction equation (13) is implemented into the frame of the Runge–Kutta time integration. In the basic code, the set of governing equations (1) is solved simultaneously with the multistage Runge–Kutta scheme

$$\vec{W}_i^{(m)} = \vec{W}_i^{(0)} + \alpha^{(m)} \cdot \Delta\vec{W}_i^{(m-1)}, \tag{19}$$

where the superscripts (m) denote the stage count with m running from 1 to the maximum number of stages, the subscripts i correspond to the location at mesh points in the flow field, $\alpha^{(m)}$ is the stage coefficient of the (m)-stage, and $\Delta\vec{W}_i^{(m-1)}$ represent the conservative residuals of continuity, momentum and energy equations evaluated with the MAPS+ discretization as in [20] using the flow variables from the previous $(m-1)$-stage. In the basic code, pressure is obtained in each stage from the equation of state (3). For the present pressure correction approach, pressure is not updated by the equation of state anymore, but the pressure correction equation (13) is solved and pressure is computed via Eq. (14). The solution of Eq. (13) and the pressure update by Eq. (14) are performed in each stage of the Runge–Kutta scheme prior to the computation of the conservative residuals $\Delta\vec{W}_i$. Using the pressure obtained from the pressure correction equation ensures that at every stage, when evaluating the conservative flux balances used in the residual computation, the constraint on the discrete divergence of the velocity field is established by solution of Eq. (13).

The pressure correction equation (13) is solved in the whole computational domain using a simple point-Jacobi method, and as a default 10 iterations are employed. Pressure is directly updated using Eq. (14), where no relaxation factor as in classical pressure correction methods [23] is used. Also note that in contrast to the SIMPLE pressure correction approach of [23], the pressure corrections are not used to compute any ''velocity corrections''. The derivation of the present pressure correction scheme was solely based on the approximate solution of the Riemann problem. This led to the establishment of a pressure correction equation, but it did not suggest any updates of velocities other than those directly obtained from the momentum equations. This is consistent with observations reported in the textbook of Noll [32], where it is found that for colocated pressure correction methods, additional ''velocity corrections'' besides the updates obtained directly from the momentum equations are unnecessary.

In the pressure correction equation and in the evaluation of residuals $\Delta\vec{W}_i$, for consistency the same space discretization has to be employed, and here the MAPS+ discretization of [20] is used. For completeness the MAPS+ discretization is given in Table 2, where the functions β^{M} and β^{P} are defined by [20]:

$$\begin{aligned} \beta^{\mathrm{M}} &= \max(0, 2 \cdot M^{\max\ 1} - 1), \quad M^{\max\ 1} = \min[\max(|M^{\mathrm{L}}|, |M^{\mathrm{R}}|), 1], \\ \beta^{\mathrm{P}} &= \max(0, 2 \cdot M^{\min\ 1} - 1), \quad M^{\min\ 1} = \min[\min(|M^{\mathrm{L}}|, |M^{\mathrm{R}}|), 1]. \end{aligned} \tag{20}$$

Note that for incompressible flows, the MAPS+ and the FDS scheme in Table 1 become identical. In order to obtain the correct scaling of dissipation in the incompressible limit, the speed of sound c in Table 2 has to be replaced by an artificial speed of sound c' [20]:

$$\begin{aligned} c' &= \sqrt{\alpha^2 q^2 + M_r^2 c^2}, \\ \alpha &= \frac{1}{2}\left(1 - M_r^2\right), \end{aligned} \tag{21}$$

where q represents the flow speed, and M_{r} is a reference Mach number defined as

Table 2
Dissipative terms of MAPS+ scheme

$$\Delta F_{\rho} = \frac{1}{c^{\max}}(1-|M_0|)\Delta p + \rho\beta^{\mathrm{M}}\Delta q_n + |q_n|\Delta\rho$$

$$\Delta F_{\rho u} = n_x\beta^{\mathrm{P}}\Delta p + \frac{1}{c^{\max}}u(1-|M_0|)\Delta p + n_x\rho^{\min}c^{\min}(1-|M_0|)\Delta q_n + \rho u\beta^{\mathrm{M}}\Delta q_n + |q_n|\Delta\rho u$$

$$\Delta F_{\rho y} = n_y\beta^{\mathrm{P}}\Delta p + \frac{1}{c^{\max}}v(1-|M_0|)\Delta p + n_y\rho^{\min}c^{\min}(1-|M_0|)\Delta q_n + \rho v\beta^{\mathrm{M}}\Delta q_n + |q_n|\Delta\rho v$$

$$\Delta F_{\rho H} = \frac{1}{c^{\max}}H^{\min}(1-|M_0|)\Delta p + \rho H\beta^{\mathrm{M}}\Delta q_n + |q_n|\Delta\rho H$$

$$|M_0| = \min(\max(|M^{\mathrm{L}}|, |M^{\mathrm{R}}|), 1)$$

$$c^{\max} = \max(c^{\mathrm{L}}, c^{\mathrm{R}})$$

$$c^{\min} = \min(c^{\mathrm{L}}, c^{\mathrm{R}})$$

$$\rho^{\min} = \min(\rho^{\mathrm{L}}, \rho^{\mathrm{R}})$$

$$H^{\min} = \min(H^{\mathrm{L}}, H^{\mathrm{R}})$$

$$u = 0.5\cdot(u^{\mathrm{L}} + u^{\mathrm{R}})$$
$$v = 0.5\cdot(v^{\mathrm{L}} + v^{\mathrm{R}})$$
$$\rho = 0.5\cdot(\rho^{\mathrm{L}} + \rho^{\mathrm{R}})$$
$$\rho u = 0.5\cdot(\rho^{\mathrm{L}}u^{\mathrm{L}} + \rho^{\mathrm{R}}u^{\mathrm{R}})$$
$$\rho v = 0.5\cdot(\rho^{\mathrm{L}}v^{\mathrm{L}} + \rho^{\mathrm{R}}v^{\mathrm{R}})$$
$$\rho H = 0.5\cdot(\rho^{\mathrm{L}}H^{\mathrm{L}} + \rho^{\mathrm{R}}H^{\mathrm{R}})$$
$\beta^{\mathrm{M}} \rightarrow$ see Eq. (20)
$\beta^{\mathrm{P}} \rightarrow$ see Eq. (20)

$$M_{\mathrm{r}}^2 = \min\left[\max\left(\frac{q^2}{c^2}, k\frac{q_\infty^2}{c_\infty^2}\right), 1\right], \tag{22}$$

with k usually set to unity. The artificial speed of sound c' is also used to compute the allowable time step.

To solve the governing equations (5) for constant density incompressible flow, in the basic Runge–Kutta time integration of Eq. (19) the density and energy components of $\vec{W}$ are not updated. To account for variations in density and temperature, an equation of temperature needs to be established. To ensure conservation properties, this temperature equation is based on changes of conservative variables. Temperature is related to the conservative variables $\vec{W}$ by

$$T = (\gamma-1)\left[\frac{\rho E}{\rho} - 0.5\cdot\frac{(\rho u)^2 + (\rho v)^2}{\rho^2}\right], \tag{23}$$

and using the chain rule temperature changes ΔT can be expressed through changes in conservative variables $\Delta\vec{W}$ as

$$\Delta T = (\gamma-1)\frac{1}{\rho}[(-E + u^2 + v^2)\cdot\Delta\rho - u\cdot\Delta(\rho u) - v\cdot\Delta(\rho v) + \Delta(\rho E)]. \tag{24}$$

With the Runge–Kutta time stepping of Eq. (19), temperature is integrated by

$$T_i^{(m)} = T_i^{(0)} + \alpha^{(m)}\cdot\Delta T_i^{m-1}. \tag{25}$$

Table 3
Number of time steps required for inviscid, incompressible flow around NACA0012 at $\alpha = 0°$ to reduce residual by eight orders of magnitude

Case	Method			
	Pressure based, no preconditioning, constant density, $M_\infty = 0.0$	Pressure based, no preconditioning, variable density, $M_\infty = 0.001$	Pressure based, preconditioning, variable density, $M_\infty = 0.001$	Density based, preconditioning, variable density, $M_\infty = 0.001$
NACA0012, $\alpha = 0°$	662	668	594	1387

Density is then updated in each stage using the equation of state (3). Note that this implementation does not allow time accurate computations, since density changes in the continuity equation were neglected in the derivation of the pressure correction equation. This is of no concern in the present work, because for steady flow computations the final steady state solution is not affected.

With this implementation, inviscid flow around the NACA0012 airfoil was computed. As computational mesh, a structured O-mesh with 160 cells around the airfoil and 32 cells in normal direction was used. Completely incompressible flow ($M_\infty = 0.0$) was computed by setting density constant, and low Mach number flow at $M_\infty = 0.001$ where density and temperature variations were taken into account by using Eq. (24). The angle of attack was chosen to $\alpha = 0°$. No multigrid acceleration was employed for the inviscid flow, and it was found that the allowable CFL-number had to be reduced from 6 to about 4. In the first two columns of Table 3, the number of time steps required to reach a convergence criterion of 10^{-8} are given for the completely incompressible, constant density flow at $M_\infty = 0.0$, and for the very low Mach number flow at $M_\infty = 0.001$. Note that as residual for the constant density flow the change of velocity was used instead of change of density. As can be seen from the table, the inclusion of temperature and density variation did not lead to a significant change in the convergence properties.

From these test cases, it may be concluded that the pressure correction approach derived above is feasible for completely incompressible, constant density and very low Mach number flows within the framework of the original compressible NOUGAT code. However, the question remains how to accomplish the transition to compressible flows in order to derive a method applicable for all speeds.

6. Extension to compressible flows

Inspection of the pressure correction equation (13) reveals that for Mach numbers $M \geqslant 1$, the left hand side of Eq. (13) vanishes, and the equation becomes undetermined and unsolvable. To prevent the left hand side going to zero with M approaching unity, a time derivative of pressure may be added to the left hand side of Eq. (13) to represent the temporal change of density in the continuity equation:

$$\frac{\partial \rho}{\partial t} = \frac{1}{c^2}\frac{\partial p}{\partial t}, \tag{26}$$

where Laplace's equation (4) was employed to express temporal changes in density by changes of pressure. The pressure correction equation (13) was basically derived from the discrete continuity equation under the constraint that divergence of velocity must be zero. Adding the time derivative of density, respectively pressure, relaxes this constraint, but the pressure correction equation is now well defined for $M \geqslant 1$. However, the pressure correction equation is still purely elliptic, which violates the nature of supersonic flow. To remedy this, one can again use the discrete continuity equation and express all terms involving density with

$$\rho = \frac{\gamma}{c^2}(p + p'), \tag{27}$$

and build the left hand side coefficients for p'. Due to the upwinding of the basic spatial discretization, this leads to an elliptic/hyperbolic equation for the pressure correction p' similar to equations derived in [12–18], where incompressible, pressure based methods were extended to compressible flows. Note that relation (26) is only valid for isentropic flows, which will however not affect the steady state solution but should only influence the convergence behavior, as was argued, e.g., in [12,13].

In order to assess the suitability of the present pressure correction approach for compressible flows, 1D flow in a Laval nozzle was computed. In order to clearly identify the capabilities and limits of the approach, only a first order implementation was investigated, and for time integration a 3-stage Runge–Kutta scheme without any acceleration techniques except local time stepping was used. Results obtained with the basic compressible code using the MAPS+ discretization [20] served as reference. Fig. 1 shows the Mach number distribution in the Laval nozzle for different values of backpressure. The case with the lowest backpressure yielding a pre-shock Mach number of about $M = 2.9$ is identical to the case used in the investigations of [20,33], where the properties of the MAPS and MAPS+ spatial discretizations were assessed. In Fig. 2, for different approaches the number of time steps required to reduce the density residual by nine orders of magnitude is displayed as a function of pre-shock Mach number. The results of the compressible, density based code are denoted by circles. For the two lower Mach number cases, the pressure based approach with the elliptic/hyperbolic pressure correction performed somewhat better than the density based approach. Note that when using the pressure correction equation (13) with the time derivative term of Eq. (26) only, the integration diverged whenever supersonic flow occurred. Only the change from elliptic to hyperbolic character using Eq. (27) established a stable integration. Due to the formulation of the temperature equation (24), the conservation properties of the basic discretization are not violated with the present pressure correction approach, and exactly the same steady state solutions as with the density based code were obtained. Thus, the good shock capturing capabilities of the MAPS+ discretization are retained for the pressure based approach.

Reduction of backpressure to achieve a pre-shock Mach number of about $M = 2.0$ led to very slow convergence of the present pressure correction approach, and even after 10,000 time steps the convergence

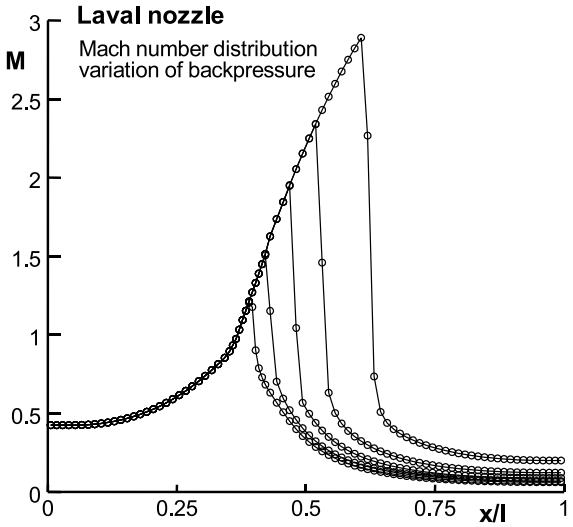

Fig. 1. Mach number distribution for variation of backpressure in 1D Laval nozzle flow.

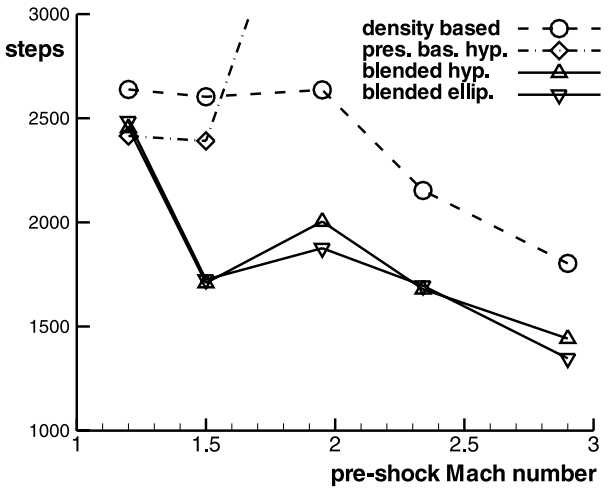

Fig. 2. Number of time steps as function of pre-shock Mach number for 1D Laval nozzle flow computed with different approaches.

criterion was not reached, as indicated by the slope of the dash-dotted line in Fig. 2. Further reduction of backpressure to increase Mach number resulted in divergence of the present pressure based approach. Neither reduction of CFL number nor introduction of pressure relaxation in Eq. (14) led to stable solutions. Due to these experiences and guided by the observation that the density based approach proved to be well suited for high speed compressible flows [20,33], in this work the purely pressure based approach was not pursued further for computation of flows at all speeds.

From the findings outlined above it became apparent that a blending from the low speed, pressure based formulation to the high speed, density based formulation should be established. Essentially, two possibilities exist: the first is to use the pressure based approach up to a certain finite Mach number, e.g., $M = 0.3$, and for Mach numbers higher than that use the density based approach. A similar technique was used in [17] to switch between the classical incompressible discretization of [21] and the compressible FDS scheme according to [19]. However, this introduces some arbitrariness in the selection of a suitable switching Mach number. Furthermore, the approximate solution of the Riemann problem, which led to the discretization summarized in Eq. (7) and Table 1, and which was also used as a guideline to derive the pressure correction equation (13), suggests otherwise and leads to the second possibility:

The actual pressure p^{act} to be used in the computation may be computed with a blending function from the dissipative terms corresponding to the approximate solution of the Riemann problem, Table 1, as

$$p^{\mathrm{act}} = (1 - |M_0|) \cdot p^{\mathrm{inc}} + |M_0| \cdot p^{\mathrm{comp}}, \tag{28}$$

where p^{inc} is the "incompressible" pressure determined from the pressure correction equation (13), and p^{comp} is the "compressible" pressure computed with the common formula

$$p = (\gamma - 1)\left[\rho E - \frac{1}{2}\rho q^2\right]. \tag{29}$$

Note that p^{inc} computed from the pressure correction enters the residual computation in the Runge–Kutta time stepping scheme. Due to the blending $(1 - |\mathrm{M}_0|) \cdot p^{\mathrm{inc}}$, this influence on the flux balances is linearly reduced to zero when the flow becomes supersonic, resulting in a purely density based scheme in such cases. Despite the fact that the "incompressible" pressure contribution is now switched off for $M \geqslant 1$, Eq. (13)

must be prevented from becoming unsolvable, and therefore at least the time derivative term defined in Eq. (26) needs to be added. In order to still enforce the divergence-free velocity field in the incompressible limit, in Eq. (26) the physical speed of sound is used, whereas for the scaling of $\Delta p'$ in Eq. (13) the artificial speed of sound c' is employed. In doing so, the influence of the time derivative term becomes negligible in the incompressible limit.

The performance of the blended pressure/density based approach for the Laval nozzle flow problems is also displayed in Fig. 2 by triangular symbols. For the formulation of the pressure correction equation, the elliptic/hyperbolic formulation employing Eqs. (26) and (27) was used as well as the purely elliptic formulation, where only the time derivative of pressure Eq. (26) was added. The blended approach required less time steps than the purely density based approach, and no problems were encountered for higher Mach number flows. The elliptic/hyperbolic pressure correction equation did not yield any advantages compared to the purely elliptic pressure correction equation, and therefore in the following only the elliptic equation was used. Due to the respect of the strong conservation form in both the pressure based and the density based approach, the blending with Eq. (28) does not lead to any inconsistencies, and all steady state results were exactly identical to those obtained with the purely density based approach.

However, this blending technique poses the problem that even at very small Mach numbers, still a very small but finite part of the "compressible" pressure needs to be computed. Without any special means, this would require very small time steps due to the acoustic eigenvalues governing the time step size. Therefore, low speed preconditioning needs to be used to enable an efficient computation. Note that this does not impair the respect of the divergence-free constraint, since in the incompressible limit only negligible fractions of the "compressible" contribution to pressure will be used, see Eq. (28). In the literature, different preconditioning matrices are proposed [7–10], and their derivation is mainly based on the reduction of the stiffness of the equations. Choi and Merkle also addressed the problem of preconditioning for viscous flows and established a suitable method [8]. As observed in [7,10], this method does not revert to the unpreconditioned case for $M \geqslant 1$, and in [7] it was viewed as preferable to eliminate the preconditioning for supersonic flows. Therefore, in the following a preconditioning matrix similar to that in [8] will be derived which yields the identity matrix for supersonic flow. Coherent with the line of argumentation used throughout this contribution, the derivation of this preconditioning matrix will be based on terms from the approximate solution of the Riemann problem using the Mach number expansion of the FDS scheme [20]. For brevity only the 1D case is regarded.

Consider the discrete 1D Euler equations discretized using Eq. (7) and Table 1 or Table 2. This leads to the system of equations

$$\begin{aligned}
&\left[(1-|M_0|)\frac{1}{c^2}\frac{\Delta p}{\Delta t}\right]+\frac{\Delta\rho}{\Delta t}+\frac{\partial(\rho u)}{\partial x}=\frac{1}{c}(1-|M_0|)\frac{\Delta^2 p}{\Delta x}+\mathrm{ODT},\\
&\left[(1-|M_0|)u\frac{1}{c^2}\frac{\Delta p}{\Delta t}\right]+\frac{\Delta(\rho u)}{\Delta t}+\frac{\partial(\rho u^2+p)}{\partial x}=u\frac{1}{c}(1-|M_0|)\frac{\Delta^2 p}{\Delta x}+\mathrm{ODT},\\
&\left[(1-|M_0|)H\frac{1}{c^2}\frac{\Delta p}{\Delta t}\right]+\frac{\Delta(\rho E)}{\Delta t}+\frac{\partial(\rho u H)}{\partial x}=H\frac{1}{c}(1-|M_0|)\frac{\Delta^2 p}{\Delta x}+\mathrm{ODT},
\end{aligned}\tag{30}$$

where on the right hand side $\Delta^2 p$ denotes second differences of pressure in the low speed pressure dissipation, and ODT denotes other dissipative terms. On the left hand side the spatial partial derivatives should denote the centrally discretized flux balances, and the time derivatives of the conservative variables are expressed as finite differences. Furthermore, one finds on the left hand side of Eq. (30) terms given in brackets which do not follow directly from Eq. (7) and Table 1 or Table 2: to all equations, appropriately scaled finite difference approximations of the time derivative of pressure were added artificially to counterbalance the spatial second derivatives of pressure on the right hand side. Consistent with the pressure

differences on the right hand side, these time derivatives are multiplied by $(1-|M_0|)$. Using Eq. (29), the change in pressure Δp may be expressed by changes of conservative variables as

$$\Delta p = (\gamma - 1)\left[\frac{q^2}{2}\Delta\rho - u\Delta(\rho u) + \Delta(\rho E)\right]. \tag{31}$$

Introducing the definition of Δp given by Eq. (31) into Eq. (30), all terms with $\Delta\rho, \Delta(\rho u), \Delta(\rho E)$ may be grouped as elements of a matrix $\overline{\overline{P}}^{-1}$. For preconditioning, the physical speed of sound c in Eq. (30) has to be replaced by the artificial speed of sound c' according to Eq. (21). Inversion of the matrix $\overline{\overline{P}}^{-1}$ formed by the changes of the conservative variables leads to a preconditioning matrix $\overline{\overline{P}}$ to directly multiply the conservative residuals. Omitting the multiplication with $(1-|M_0|)$ on the left hand side in Eq. (30), this matrix becomes similar to the preconditioning matrix of Choi and Merkle, as was observed already in [34]. However, in [34] no use was made of this connection to obtain a preconditioning matrix directly for multiplication of the conservative residuals. Multiplication of the pressure changes by $(1-|M_0|)$ reduces the influence of preconditioning to zero for $M \geqslant 1$. The inversion of the matrix $\overline{\overline{P}}^{-1}$ obtained from Eq. (30) is easily achieved, and the extension to higher dimensions is straightforward. The matrix $\overline{\overline{P}}^{-1}$ and its inverse, the preconditioning matrix $\overline{\overline{P}}$, are given in Table 4 for 3D application. Note the ordering of variables in the vector of conservative variables $\vec{W}$, which deviates from the conventional ordering. This ordering enables an easy extension from the 1D case to higher dimensions, however the conservative residuals have to be ordered in the same way before multiplication.

In Table 3, also the number of time steps required for convergence using the pressure correction approach with and without preconditioning for the computation of flow around the NACA0012 airfoil at $M_\infty = 0.001$ and $\alpha = 0°$ is given. From these results it is concluded that the pressure correction approach also works well in combination with preconditioning.

7. Application of the method

First, the developed method was applied to the computation of inviscid flow fields. In order to check the consistency and functionality of the blending technique between pressure and density based approach, a grid refinement study for a variety of Mach numbers was performed. For the NACA0012 airfoil at $\alpha = 0°$, free-stream Mach number was varied from $M_\infty = 0.001$ to $M_\infty = 0.85$, and computations were performed on meshes with 40×8, 80×16, and 160×32 cells. For comparison the purely pressure based approach established in Section 5, the blended approach of Section 6, and the basic compressible, density based approach were investigated. In all cases the preconditioning matrix of Table 4 was used, and for pressure correction the elliptic equation (13) with added time derivative (26) was employed throughout. Fig. 3 displays surface pressure distributions obtained on the finest mesh for selected Mach numbers, which illustrate the change in the flow characteristics. To assess the consistency of the three investigated methods, drag coefficients computed on successively refined meshes for increasing free-stream Mach number are listed in Table 5. Up to a free-stream Mach number of $M_\infty = 0.7$, the flow remained completely subsonic, and the exact drag coefficient should be zero. As can be seen from Table 5, with mesh refinement the error in drag is reduced by approximately a factor of 4, consistent with second order accuracy of the numerical method. The steady state results from all three methods investigated were exactly identical on all three meshes for all Mach numbers, therefore only one set of results is listed. The fact that the steady state results of the different approaches are identical at steady state was already observed for the 1D Laval nozzle flow, and the mesh refinement investigation performed in 2D gives additional proof of the consistency of the blending technique.

Table 4
Preconditioning matrix for conservative residuals

Definitions (note ordering of equations in vector of conservative variables $\vec{W}$)

$$\vec{W} = \begin{bmatrix} \rho \\ \rho E \\ \rho u \\ \rho v \\ \rho w \end{bmatrix}, \quad q^2 = u^2 + v^2 + w^2, \quad c^2 = \gamma \frac{p}{\rho}, \quad h = 0.5 \cdot q^2 + \frac{c^2}{\gamma - 1}$$

$$\Theta = (1 - |M_0|) \cdot \frac{\gamma - 1}{c'}, \quad |M_0| \rightarrow \text{see Eq. (8)}, \quad c' \rightarrow \text{see Eq. (21)}$$

Matrix resulting from addition of pressure time derivative (see Eq. (30))

$$\overline{\overline{P}}^{-1} = \begin{bmatrix} 0.5 \cdot \Theta q^2 + 1 & \Theta & -\Theta u & -\Theta v & -\Theta w \\ 0.5 \cdot \Theta q^2 h & \Theta h + 1 & -\Theta u h & -\Theta v h & -\Theta w h \\ 0.5 \cdot \Theta q^2 u & \Theta u & -\Theta u^2 + 1 & -\Theta v u & -\Theta w u \\ 0.5 \cdot \Theta q^2 v & \Theta v & -\Theta u v & -\Theta v^2 + 1 & -\Theta w v \\ 0.5 \cdot \Theta q^2 w & \Theta w & -\Theta u w & -\Theta v w & -\Theta w^2 + 1 \end{bmatrix}$$

Preconditioning matrix for multiplication of conservative residuals

$$\overline{\overline{P}} = \frac{1}{\Theta(h - 0.5q^2)} * \begin{bmatrix} \Theta(h - q^2) + 1 & -\Theta & \Theta u & \Theta v & \Theta w \\ -0.5 \cdot \Theta q^2 h & -0.5 \cdot \Theta q^2 + 1 & \Theta u h & \Theta v h & \Theta w h \\ -0.5 \cdot \Theta q^2 u & -\Theta u & \Theta(0.5 \cdot q^2 + h - v^2 - w^2) + 1 & \Theta v u & \Theta w u \\ -0.5 \cdot \Theta q^2 v & -\Theta v & \Theta u v & \Theta(0.5q^2 + h - u^2 - w^2) + 1 & \Theta w v \\ -0.5 \cdot \Theta q^2 w & -\Theta w & \Theta u w & \Theta v w & \Theta w(0.5q^2 + h - u^2 - v^2) + 1 \end{bmatrix}$$

The convergence behavior of the present method can be assessed from Fig. 4, where the time steps required to reduce the density residual by eight orders of magnitude on the finest mesh are displayed as a function of free-stream Mach number. For the density based approach, the CFL number was set to CFL = 6, for the blended approach to CFL = 3.5, and for the purely pressure based approach, up to a free-stream Mach number of $M_\infty = 0.2$ also CFL = 3.5 could be used, and with increasing free-stream Mach number the CFL number had to be reduced successively to CFL = 1.5 . Several observations can be made from Fig. 4. The pressure based approach converged significantly faster for low Mach number flows than the density based approach, despite the lower CFL number, see also Table 3. Solving the pressure correction equation, for Mach numbers above $M_\infty = 0.2$ the number of time steps required increased, especially for the purely pressure based approach. Using the density based approach the number of time steps remained almost constant for free-stream Mach numbers below $M_\infty = 0.5$. At $M_\infty = 0.5$, the purely pressure based approach lost its attractiveness due to the steep increase in the number of time steps required at higher free-stream Mach numbers. For the transonic cases, convergence of this approach severely degenerated, and for $M_\infty = 0.85$ even after 10,000 time steps the convergence criterion was not met, indicated by the dash-dotted line in Fig. 4. The blended pressure/density based method combined the strengths of pressure and density based approaches: for incompressible and low Mach number flows it yielded the efficiency of the pressure based method, for higher Mach number subsonic flows it still offered some advantage compared to the density based approach, and for the transonic cases it only slightly degraded with respect to the density based approach.

In the next case the robustness of the method was to be assessed. For the inviscid, incompressible flow around the NACA0012, the angle of attack was increased from $\alpha = 12°$ to $\alpha = 14°$ and $\alpha = 16°$. The corresponding convergence histories are shown in Figs. 5 and 6. For $\alpha = 14°$, reasonable convergence was

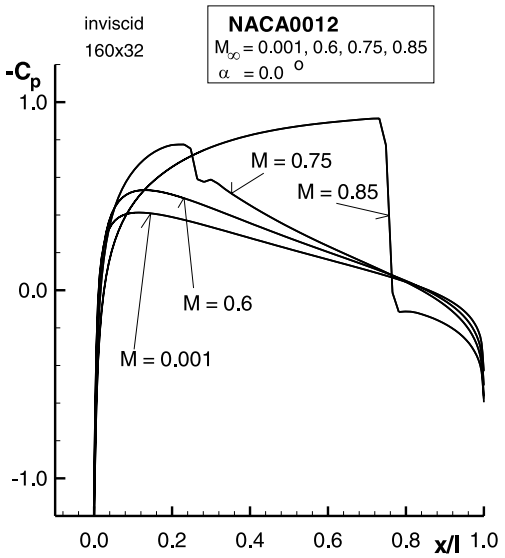

Fig. 3. Surface pressure distribution for Mach number variation of inviscid flow around NACA0012 airfoil at $\alpha = 0°$.

Table 5
Computed drag coefficient as function of Mach number and grid refinement for inviscid flow around NACA0012 at $\alpha = 0°$

Grid	M										
	0.001	0.01	0.1	0.2	0.3	0.4	0.5	0.6	0.7	0.75	0.85
40×8	.01875	.01875	.01882	.01906	.01950	.02021	.02135	.02300	.02549	.02776	.06780
80×16	.00482	.00482	.00483	.00487	.00493	.00502	.00517	.00541	.00578	.00615	.05286
160×32	.00096	.00096	.00096	.00096	.00096	.00097	.00097	.00098	.00099	.00103	.04748

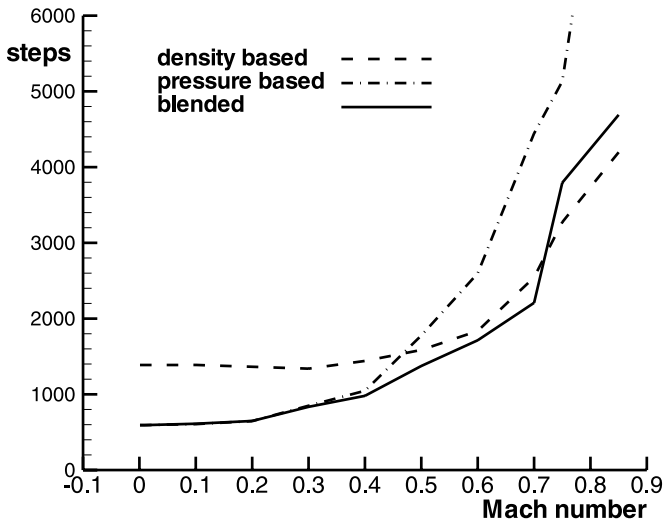

Fig. 4. Number of time steps as function of free-stream Mach number for inviscid flow around NACA0012 airfoil computed with different approaches.

achieved, for $\alpha = 16°$ the residual decreased only very slowly and oscillatory, and total lift exhibited also oscillations, which however die out. The same case was run without the pressure correction approach but with the basic preconditioned, density based scheme. As can be seen in Fig. 7, increasing the angle of attack from $\alpha = 13°$ to 13.5° destroyed the convergence of the scheme. In Figs. 8 and 9 the pressure distributions for $\alpha = 12°$–16° are displayed, where Fig. 9 shows an enlargement of the trailing edge region. Increasing the angle of attack beyond 12° brought the inviscid flow closer to separation. This separation was solely triggered by the inherent numerical dissipation, it occured earlier on coarser meshes and later on finer

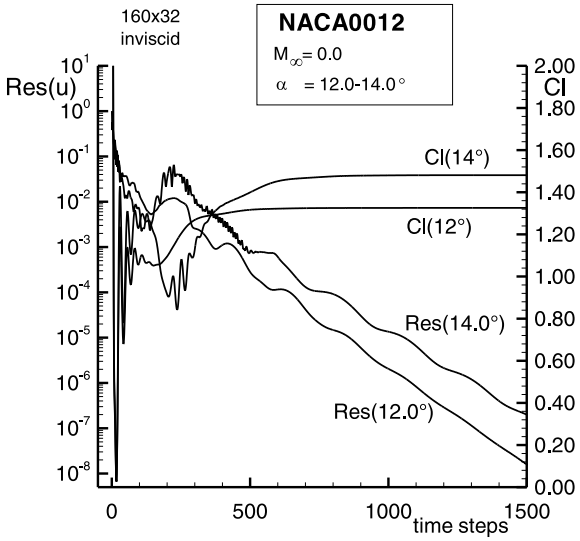

Fig. 5. Convergence for inviscid, incompressible flow around NACA0012 airfoil at $\alpha = 12°$–14° with blended pressure based method.

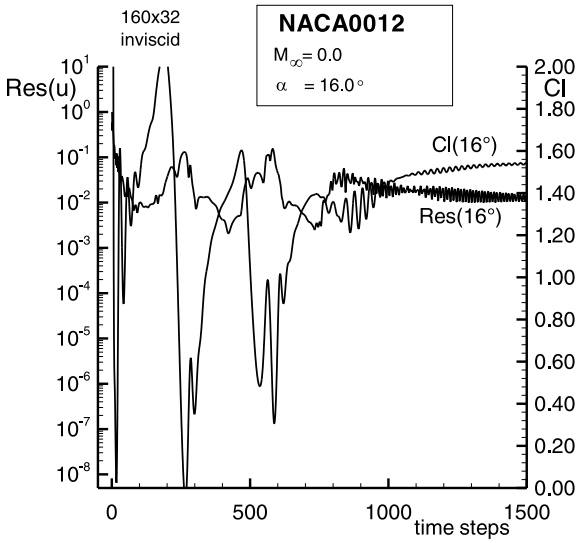

Fig. 6. Convergence for inviscid, incompressible flow around NACA0012 airfoil at $\alpha = 16°$ with blended pressure based method.

meshes. No physical arguments hold for the occurrence of separation, it is completely of numerical nature. The respect of the divergence-free velocity field is assumed to become crucial close to separation, and due to the lack of any means to enforce this constraint, the basic preconditioned, density based method failed for the computation of such flows.

In the next test cases, the computation of viscous flow around the RAE2822 airfoil at $M_\infty = 0.0$ and $\alpha = 8°$ was considered using a hybrid mesh. The hybrid mesh was identical to the mesh used in [30] and

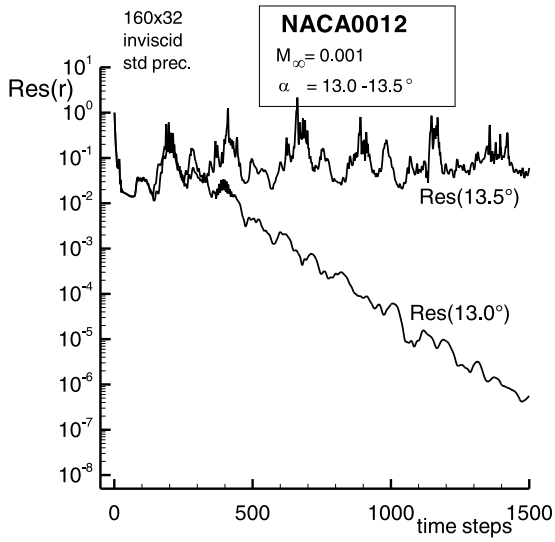

Fig. 7. Convergence for inviscid, incompressible flow around NACA0012 airfoil at $\alpha = 13°$–$13.5°$ with preconditioned density based method.

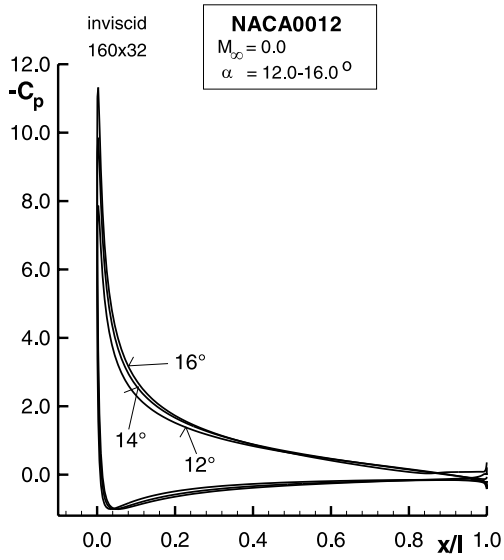

Fig. 8. Pressure distributions for inviscid, incompressible flow around NACA0012 airfoil at $\alpha = 12°$–$16°$.

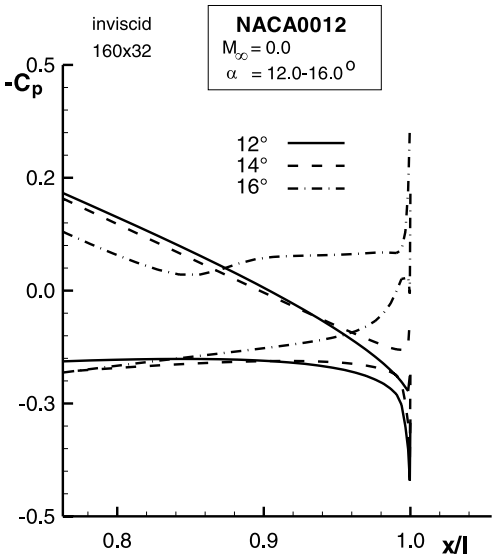

Fig. 9. Pressure distributions for inviscid, incompressible flow around NACA0012 airfoil at $\alpha = 12°$–$16°$, enlargement at trailing edge.

consisted of about 23,000 quadrilateral and triangular cells, where the 4800 quadrilateral cells were used in the vicinity of the airfoil to resolve the viscous region, with 192 of these cells located directly on the airfoil surface. A 4-level agglomeration multigrid was used to accelerate convergence, and the influence of turbulence was modeled following Spalart and Allmaras [31]. In Table 6, the number of multigrid cycles required to drive the residual down by five orders of magnitude is given. Additionally, results are listed for the computation of the same configuration at $M_\infty = 0.001$ with and without preconditioning. As can be seen from Table 6, convergence for these cases was not as favorable as for the $M = 0$ case. This may be explained by the fact that for $M_\infty = 0.0$ the residual was computed from changes of velocity, which were set to zero on the solid surface. For the cases at $M_\infty = 0.001$, the residual was based on the change of density, which was computed also on the solid surface. Here the largest residuals occurred always at the trailing edge, thus deteriorating convergence. In order to test the applicability of the blending technique to compressible flow, the free-stream conditions were changed to $M_\infty = 0.73$ and $\alpha = 2.8°$. Fig. 10 shows that the convergence of the new method is comparable to that of the standard compressible code, despite the fact that only a CFL number of 4 was used. The corresponding pressure distribution is displayed in Fig. 11. The results are identical to those obtained with the compressible, density based code, which is also indicated by the convergence to the same final lift coefficient in Fig. 10. The results correspond to results obtained with the DLR-τ code [35].

Table 6
Number of multigrid cycles required for viscous, incompressible flow around RAE2822 at $\alpha = 8°$ to reduce residual by five orders of magnitude

Case	Method			
	Pressure based, no preconditioning, constant density, $M_\infty = 0.0$	Pressure based, no preconditioning, variable density, $M_\infty = 0.001$	Pressure based, preconditioning, variable density, $M_\infty = 0.001$	Density based, preconditioning, variable density, $M_\infty = 0.001$
RAE2822, $\alpha = 8°$	258	450	285	338

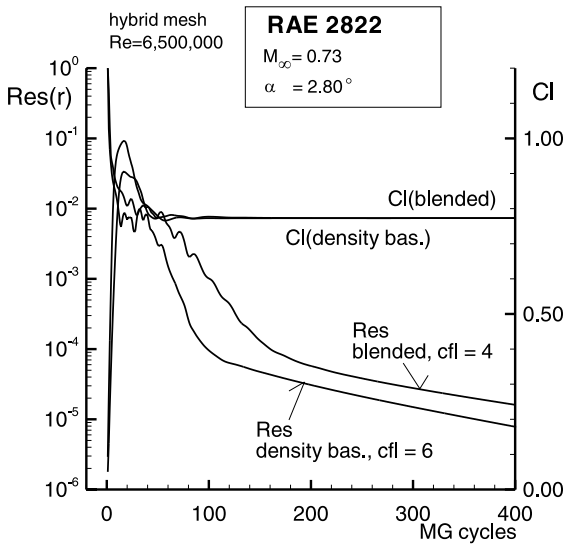

Fig. 10. Convergence for viscous, compressible flow around RAE2822 airfoil computed with blended pressure based method and density based method.

To asses the robustness of the method for incompressible flow, similarly to the inviscid computations the angle of attack was increased, here from $\alpha = 8°$ to $\alpha = 11.25°$. As can be seen from Fig. 12, using the default value of 10 Jacobi iterations for the solution of the pressure correction equation, the computation did not converge. Boldly increasing this number to 100 iterations however led to convergence. This behavior is assumed to be triggered by the very large cell aspect ratios close to the solid surface, thus severely increasing the stiffness of the pressure correction equation. Application of the preconditioned, density based method did not lead to convergence, Fig. 13. The difficulties in computing this case can again be traced back to the onset of separation, as is visible in the pressure distributions shown in Figs. 14 and 15.

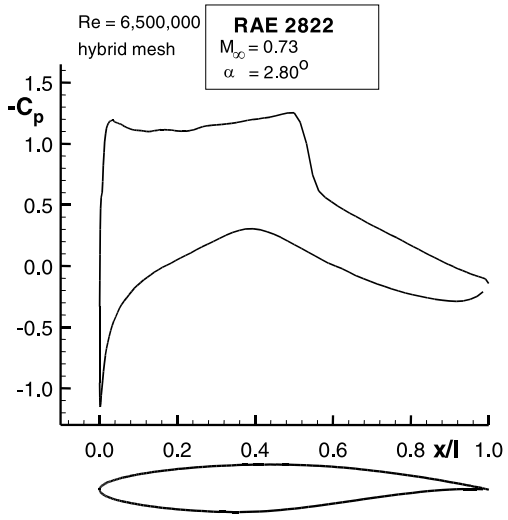

Fig. 11. Pressure distribution for viscous, compressible flow around RAE2822 airfoil.

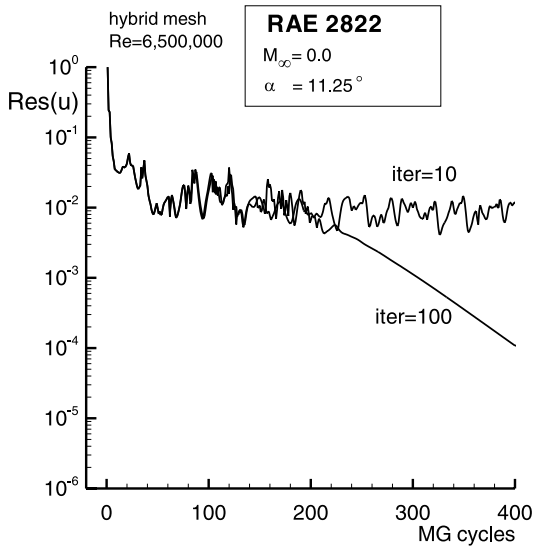

Fig. 12. Convergence for viscous, incompressible flow around RAE2822 airfoil computed with blended pressure based method using 10 and 100 Jacobi iterations.

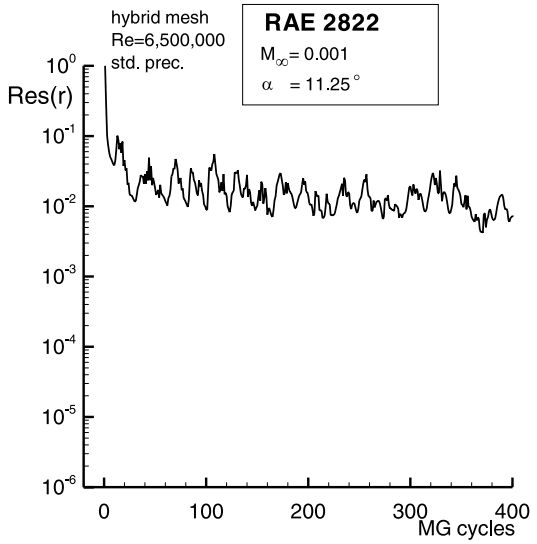

Fig. 13. Convergence for viscous, incompressible flow around RAE2822 airfoil computed with preconditioned density based method.

8. Conclusion

A pressure correction equation was derived from the approximate solution of the Riemann problem at low speeds, and parallels to classical incompressible methods were drawn. The derivation was mainly based on the observation that for incompressible flows, the velocity field has to be divergence-free, and to enforce this constraint a corresponding pressure field needs to be established. Due to the consistent derivation from

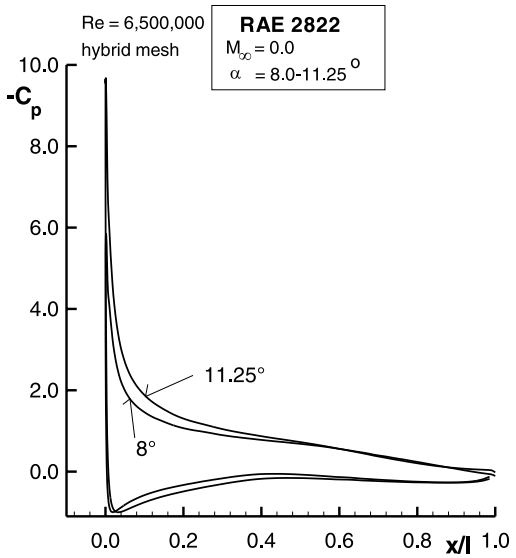

Fig. 14. Pressure distributions for viscous, incompressible flow around RAE2822 airfoil close to separation.

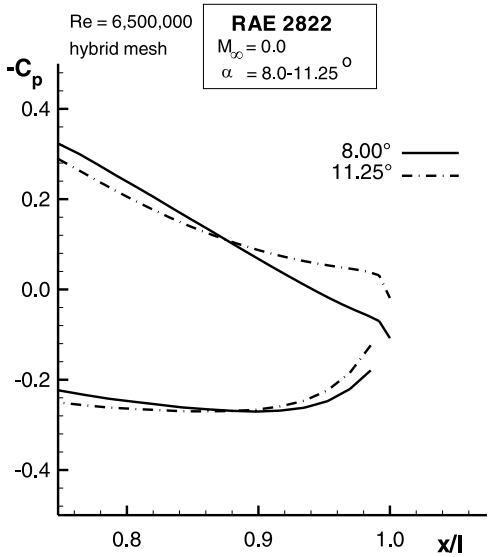

Fig. 15. Pressure distributions for viscous, incompressible flow around RAE2822 airfoil close to separation, enlargement at trailing edge.

the approximate solution of the Riemann problem, the incorporation into the framework of a compressible code was straightforward, and completely incompressible flow at $M_\infty = 0.0$ could be computed. In order to allow the computation of flows with mixed incompressible/compressible regions, a suitable blending technique was developed for the transition from the pressure based, incompressible method to the density based, compressible method. The blending functions were also derived from the approximate solution of

the Riemann problem. The blending reflects the change in the character of the unsteady equations from elliptic/hyperbolic for incompressible flows to purely hyperbolic for compressible flows. It was found necessary to use preconditioning with this blending technique to account for a remaining "compressible" contribution in the incompressible limit, and a suitable matrix directly applicable to conservative residuals was derived. The blended pressure based approach allowed to exploit the advantages of the separate solution of the continuity equation to establish the divergence-free constraint. This led to improved convergence and robustness for incompressible flows. The blending to a density based scheme with increasing Mach number retained the robustness and accurate shock capturing capabilities of such methods for high speed flows.

With this work, a coherent framework was established to cover the discretization of both incompressible and compressible flows: the derivation of a pressure correction equation, the establishment of a suitable preconditioning matrix, and the formulation of a flux splitting scheme for all speeds were consistently based on the expansion of the classical FDS scheme in terms of Mach number [20].

Future work needs to be directed to an improvement of the method used to solve the pressure correction equation. The simple point-Jacobi iteration used here for conceptual investigations degrades considerably for high aspect ratio meshes and thus impairs the benefit possibly to be achieved by the solution of this equation.

Acknowledgements

Parts of this study were conducted when the author was in residence at the Institute for Computer Applications in Science and Engineering, ICASE, and the author expresses his thanks to Dr. Manuel Salas, ICASE Director, for providing this opportunity.

References

[1] V.N. Vatsa, M.D. Sanetrik, E.B. Parlette, Development of a flexible and efficient multigrid-based flow solver (unpublished), AIAA Paper 93-0677, 1993.
[2] D.J. Mavriplis, A three-dimensional multigrid Reynolds-averaged Navier–Stokes solver on unstructured meshes, AIAA J. 30 (1995) 445–453.
[3] T. Gerhold, O. Friedrich, J. Evans, M. Galle, Calculation of complex three-dimensional configurations employing the DLR TAU code (unpublished), AIAA Paper 97-0167, 1997.
[4] D.C. Jespersen, T.H. Pulliam, P.G. Buning, Recent enhancements to OVERFLOW (unpublished), AIAA Paper 97-0644, 1997.
[5] S. Krist, R. Biedron, C. Rumsey, CFL3D User's Manual (Version 5.0), NASA TM-1998-208444, 1998.
[6] N. Kroll, C.-C. Rossow, K. Becker, F. Thiele, The MEGAFLOW project, Aerospace Sci. Technol. 4 (2000) 223–237.
[7] E. Turkel, Preconditioning techniques in computational fluid dynamics, Annu. Rev. Fluid Mech. 31 (1999) 385–416.
[8] Y.-H. Choi, C.L. Merkle, The application of preconditioning to viscous flows, J. Comput. Phys. 105 (1993) 207–223.
[9] J.M. Weiss, W.A. Smith, Preconditioning applied to variable and constant density flows, AIAA J. 33 (1995) 2050–2057.
[10] D.L. Darmofal, B. Van Leer, Local preconditioning: manipulating mother nature to fool father time, in: D. Caughey, M. Hafez (Eds.), Computing the Future 2: Computational Fluid Dynamics and Transonic Flow, 1998.
[11] R. Rudnik, S. Melber, A. Ronzheimer, O. Brodersen, Three-Dimensional Navier–Stokes Simulations for transport aircraft high lift configurations, AIAA J. 38 (5) (2001) 895–903.
[12] K.C. Karki, S.V. Patankar, Pressure based calculation procedure for viscous flows at all speed in arbitrary configurations, AIAA J. 27 (1989) 1167–1174.
[13] I. Demirdzic, Z. Lilek, M. Peric, A colocated finite volume method for predicting flows at all speeds, Int. J. Numer. Meth. Fluids 16 (1993) 1029–1050.
[14] G. Zhou, L. Davidson, A pressure-based euler scheme for transonic internal and external flows, Comp. Fluid Dyn. 5 (1995) 169–188.
[15] S.M.H. Karimian, G.E. Schneider, Pressure-Based control-volume finite element method for flow at all speeds, AIAA J. 33 (1995) 1611–1618.
[16] H. Bijl, P. Wesseling, A unified method for computing incompressible and compressible flows in boundary fitted coordinates, J. Comput. Phys. 141 (1998) 153–177.

[17] S.R. Mathur, J.Y. Murthy, All speed flows on unstructured meshes using a pressure correction approach (unpublished), AIAA Paper 99-3365, 1999.
[18] F.-S. Lien, A pressure-based unstructured grid method for all-speed flows, Int. J. Numer. Methods Fluids 33 (2000) 355–374.
[19] P.L. Roe, Approximate Riemann solvers, parameter vectors and difference schemes, J. Comput. Phys. 43 (1981) 357–372.
[20] C.-C. Rossow, A flux splitting scheme for compressible and incompressible flows, J. Comput. Phys. 164 (2000) 104–122.
[21] C.M. Rhie, W.L. Chow, Numerical study of the turbulent flow past an airfoil with trailing edge separation, AIAA J. 21 (11) (1983) 1525–1532.
[22] H. Guillard, C. Viozat, On the behaviour of upwind schemes in the low Mach number limit, Comput. & Fluids 28 (1999) 63–86.
[23] S.V. Patankar, Numerical heat transfer and fluid flow, McGraw-Hill, New York, 1980.
[24] C. Hirsch, Numerical Computation of Internal and External Flows, Wiley, Chichester/NewYork/Brisbane/Toronto/Singapore, 1990.
[25] S.W. Armfield, Ellipticity, accuracy, and convergence of the discrete Navier–Stokes equations, J. Comput. Phys. 114 (1994) 176–184.
[26] Th. Pulliam, Artificial dissipation models for the euler equations (unpublished), AIAA Paper 85-0438, 1985.
[27] J.H. Ferziger, M. Peric, Computational Methods for Fluid Dynamics, third ed., Springer, Berlin, Heidelberg, NewYork, 2002, ISBN 3-540-42074-6.
[28] W.K. Anderson, D.L. Bonhaus, An implicit upwind algorithm for computing turbulent flows on unstructured grids, Comput. & Fluids 23 (1) (1994) 1–21.
[29] A. Haselbacher, J. Blazek, Accurate and efficient discretization of Navier–Stokes equations on mixed grids, AIAA J. 38 (2000) 2094–2102.
[30] C.-C. Rossow, Convergence acceleration on unstructured meshes, in: Contributions to the 12th STAB/DGLR Symposium Stuttgart 2000, Notes on Numerical Fluid Mechanics, vol. 77, Springer, Berlin/Heidelberg/NewYork, 2002, pp. 304–311.
[31] P.R. Spalart, S.R. Allmaras, A one-equation turbulence model for aerodynamic flows, La Recherche Aerospatiale 1 (1994) 5–21.
[32] B. Noll, Numerische Strömungsmechanik, Springer, Berlin/Heidelberg/NewYork, 1993, ISBN 3-540-56712-7.
[33] C.-C. Rossow, A simple flux-vector splitting scheme for compressible flows, in: Contributions to the 11th STAB/DGLR Symposium Berlin 1998, Notes on Numerical Fluid Mechanics, vol. 72, Vieweg, Braunschweig, Wiesbaden, 1999, pp. 355–362.
[34] R. Radespiel, E. Turkel, N. Kroll, Assessment of preconditioning methods, DLR-Forschungsbericht, FB 95-29, 1995.
[35] D. Schwamborn, T. Gerhold, V. Hannemann, On the validation of the DLR-TAU Code, in: Contributions to the 11th STAB/DGLR Symposium Berlin 1998, Notes on Numerical Fluid Mechanics, vol. 72, Vieweg, Braunschweig, Wiesbaden, 1999, pp. 426–433.